arXiv:1609.05226v1 [astro-ph.HE] 8 Aug 2016

Simulations of Energetic Particles Interacting with Nonlinear Anisotropic Dynamical Turbulence

M. Heusen & A. Shalchi

Department of Physics and Astronomy, University of Manitoba, Winnipeg, Manitoba R3T 2N2, Canada

andreasm4@yahoo.com

Received _____; accepted _____

ABSTRACT

We investigate test-particle diffusion in dynamical turbulence based on a numerical approach presented before. For the turbulence we employ the nonlinear anisotropic dynamical turbulence model which takes into account wave propagation effects as well as damping effects. We compute numerically diffusion coefficients of energetic particles along and across the mean magnetic field. We focus on turbulence and particle parameters which should be relevant for the solar system and compare our findings with different interplanetary observations. We vary different parameters such as the dissipation range spectral index, the ratio of the turbulence bendover scales, and the magnetic field strength in order to explore the relevance of the different parameters. We show that the bendover scales as well as the magnetic field ratio have a strong influence on diffusion coefficients whereas the influence of the dissipation range spectral index is weak. The best agreement with solar wind observations can be found for equal bendover scales and a magnetic field ratio of $\delta B/B_0 = 0.75$.

Subject headings: diffusion – magnetic fields – turbulence

1. Introduction

It is well-known that magnetic turbulence influences the motion of electrically charged energetic particles such as cosmic rays. Turbulence in general has different properties such as the spectrum describing how the magnetic energy is distributed among different length scales. Another fundamental aspect of turbulence is spectral anisotropy describing how magnetic turbulence varies in different directions of space. Diffusion of particles along the mean magnetic field, for instance, is controlled by gyro-resonant interactions (see, e.g., Schlickeiser 2002 and Shalchi 2009 for reviews). Therefore, the spectrum of turbulence at a certain scale or wavenumber determines the diffusion coefficient of the energetic particles with a certain energy. It should be emphasized, however, that nonlinear effects can be important for parallel diffusion and non-resonant interactions can influence the diffusion parameter in certain parameter regimes (see Shalchi 2009 for a review). Spectral anisotropy can also have an effect but this effect is weaker than originally thought (see Hussein et al. 2015). For perpendicular diffusion, however, the details of the turbulence seem to be less important because the perpendicular diffusion coefficient depends only on the so-called Kubo number and the parallel diffusion coefficient (see Shalchi 2015). Due to the latter dependence, however, the perpendicular diffusion parameter indirectly also depends on spectrum and spectral anisotropy.

Another important turbulence property is the dynamics describing the characteristic time scales over which the turbulent magnetic field decorrelates. Different approaches have been proposed in the past to model the turbulence dynamics. Some attempts are based on plasma wave propagation models in which the propagation effect itself is taken into account as well as various damping effects (see again Schlickeiser 2002 for a review). Or there is the important work of Bieber et al. (1994) in which simple models have been proposed to approximate the temporal decorrelation of turbulence, namely the so-called *damping model*

of dynamical turbulence and the *random sweeping model*. In the recent years scientists achieved a more complete understanding of the turbulence time scales. Therefore a more advanced model for the turbulence dynamics has been proposed in Shalchi et al. (2006). This model is called the *Nonlinear Anisotropic Dynamical Turbulence (NADT) model* and takes into account wave propagation effects as well as damping effects. It is the aim of this article to simulate energetic particle motion in this type of turbulence and to explore the influence of different turbulence parameters.

It was shown in different papers that dynamical turbulence effects can have a strong influence on the transport of energetic particles. This concerns parallel diffusion (see, e.g., Bieber et al. 1994) but also perpendicular diffusion (see, e.g., Shalchi et al. 2006). Such previous investigations were based on quasilinear and nonlinear calculations. These days, however, one can also obtain diffusion parameters from test-particle simulations. Previous work of this type was mostly done for magnetostatic turbulence (see, e.g., Giacalone & Jokipii 1999, Qin et al. 2002a, and Qin et al. 2002b) or undamped propagating plasma waves (see, e.g., Michałek & Ostrowski 1996 and Tautz & Shalchi 2013). In Hussein & Shalchi (2016) we have started to simulate test-particle transport in the dynamical turbulence models used in Bieber et al. (1994), namely in the *damping model of dynamical turbulence* and the *random sweeping model*. It was shown in Hussein & Shalchi (2016) that for certain turbulence parameters we can indeed reproduce different solar wind observations.

It is the purpose of the current paper to simulate particle transport in the more realistic NADT model and to compute the parallel mean free path $\lambda_{\parallel}$, the perpendicular mean free path $\lambda_{\perp}$, and the ratio of the two mean free paths $\lambda_{\perp}/\lambda_{\parallel}$. As in Hussein & Shalchi (2016) our findings are compared with the Palmer (1982) consensus range, observations of Jovian electrons (see Chenette et al. 1977), and Ulysses measurements of Galactic protons (see Burger et al. 2000). We also explore how the different turbulence parameters influence the

different diffusion parameters.

The reminder of the paper is organized as follows. In Section 2 we explain the physics of turbulence in general but we focus on the NADT model used in the current paper. The methodology which is used to perform particle transport simulations in dynamical turbulence is explained in Section 3. In Section 4 we show our numerical results obtained for parallel and perpendicular diffusion coefficients and we compare them with different solar wind observations. In Section 5 we conclude and summarize.

2. Dynamical Turbulence

2.1. Description of Magnetic Turbulence

In the analytical description of turbulence, the fundamental quantity is the magnetic correlation tensor in the wave vector space. The components of the latter tensor are defined via

$$P_{mn}\left(\vec{k},t\right)=\left\langle \delta B_m\left(\vec{k},t\right)\delta B_n^*\left(\vec{k},0\right)\right\rangle \tag{1}$$

where we have used the ensemble average operator $\langle\ldots\rangle$. A standard assumption in the theory of dynamical turbulence is that all tensor components obey the same temporal behavior and, therefore, they can be written as

$$P_{mn}\left(\vec{k},t\right)=P_{mn}\left(\vec{k}\right)\Gamma\left(\vec{k},t\right). \tag{2}$$

Here we have used the magnetostatic tensor components $P_{mn}(\vec{k})$ and the *dynamical correlation function* $\Gamma(\vec{k},t)$. In the current paper we employ the NADT model in order to approximate the function $\Gamma(\vec{k},t)$. Before we discuss this model in detail, we focus on the static tensor components.

2.2. Two-Component Turbulence

The slab/2D composite model is widely used in the transport theory of energetic particles (see, e.g., Bieber et al. 1994 and Bieber et al. 1996). In the current paper we employ this model, which is also known as two-component model, as it was already done in Hussein & Shalchi (2016). This type of turbulence description is supported by observations in the solar wind (see, e.g., Matthaeus et al. 1990, Osman and Horbury 2009a, Osman and Horbury 2009b, Turner et al. 2012), turbulence simulations (see, e.g., Oughton et al. 1994, Matthaeus et al. 1996, Shaikh and Zank 2007) as well as analytical treatments of turbulence (see, e.g., Zank and Matthaeus 1993). More details concerning the used model can be found in the aforementioned articles or in the corresponding diffusion theory papers (see, e.g., Hussein et al. (2015) and Hussein & Shalchi (2016)).

Within the two-component approximation, the components of the static correlation tensor are written as

$$P_{mn} = P_{mn}^{slab} + P_{mn}^{2D} \tag{3}$$

where we have used the components of the slab tensor

$$P_{mn}^{slab}(\vec{k}) = g^{slab}(k_{\parallel})\frac{\delta(k_{\perp})}{k_{\perp}}\delta_{mn}, \tag{4}$$

and the components of the two-dimensional tensor

$$P_{mn}^{2D}(\vec{k}) = g^{2D}(k_{\perp})\frac{\delta(k_{\parallel})}{k_{\perp}}\left(\delta_{mn} - \frac{k_m k_n}{k_{\perp}^2}\right), \tag{5}$$

with $m, n = x, y$. Furthermore, we have $P_{mz} = P_{zn} = P_{zz} = 0$ in both cases due to $\delta B_z = 0$. For the two-dimensional modes, the latter assumption is motivated by the fact that in the solar wind the power in parallel fluctuations is small in the inertial range (see Belcher & Davis 1971). For the slab modes $\delta B_z = 0$ is a consequence of the solenoidal constraint $\nabla \cdot \vec{B} = 0$.

In Eqs. (4) and (5) we have used the slab spectrum $g^{slab}(k_\parallel)$ as well as the two-dimensional (2D) spectrum $g^{2D}(k_\perp)$, respectively. For the former spectrum we employ the form

$$\begin{aligned} g^{slab}(k_\parallel) &= \frac{C(s)}{2\pi} l_{slab} \delta B^2_{slab} \\ &\times \begin{cases} (1+k_\parallel^2 l_{slab}^2)^{-s/2} & \text{if} \quad k_\parallel \leq k_d \\ (1+k_d^2 l_{slab}^2)^{-s/2} (k_d/k_\parallel)^p & \text{if} \quad k_\parallel \geq k_d \end{cases} \end{aligned} \tag{6}$$

as proposed in Bieber et al. (1994). Here we have used the slab bendover scale l_{slab}, the dissipation wavenumber k_d, the inertial range spectral index s, and the dissipation range spectral index p. Furthermore, we have employed the normalization function

$$C(s) = \frac{\Gamma\left(\frac{s}{2}\right)}{2\sqrt{\pi}\Gamma\left(\frac{s-1}{2}\right)} \tag{7}$$

with the Gamma function $\Gamma(z)$. The spectrum is correctly normalized as long as $s > 1$.

For the two-dimensional spectrum we use an extension of the model proposed by Bieber et al. (1994). By combining the spectrum used in the latter paper with the ideas discussed in Matthaeus et al. (2007) and Shalchi & Weinhorst (2009), we propose the form

$$\begin{aligned} g^{2D}(k_\perp) &= \frac{2D(s,q)}{\pi} l_{2D} \delta B^2_{2D} \\ &\times \begin{cases} \frac{(k_\perp l_{2D})^q}{(1+k_\perp^2 l_{2D}^2)^{(s+q)/2}} & \text{if} \quad k_\perp \leq k_d \\ \frac{(k_d l_{2D})^q}{(1+k_d^2 l_{2D}^2)^{(s+q)/2}} \left(\frac{k_d}{k_\perp}\right)^p & \text{if} \quad k_\perp \geq k_d. \end{cases} \end{aligned} \tag{8}$$

The only parameter which is different compared to the slab spectrum, is the energy range spectral index q controlling the spectral shape at large turbulence scales. Furthermore, we have used the extended normalization function

$$D(s,q) = \frac{\Gamma\left(\frac{s+q}{2}\right)}{2\Gamma\left(\frac{s-1}{2}\right)\Gamma\left(\frac{q+1}{2}\right)} \tag{9}$$

with $s > 1$ and $q > -1$. Eqs. (7) and (9) are linked via $C(s) = D(s, q = 0)$. In Tables 1 and 2 we list the values we have used in our simulations for the different turbulence and

particle parameters. In Fig. 1 we visualize the used spectra for slab and two-dimensional modes, respectively.

A spacial aspect of the two-component model used here is that we assume that there are no fluctuations parallel to the mean field $\delta B_z = 0$. More recent observations (see, e.g., Alexandrova et al. 2008) and numerical simulations (see, e.g., Howes et al. 2008) show an increased level of magnetic compressibility at small scales. In Hussein et al. (2015) the influence of different magnetostatic turbulence models on the parallel and perpendicular diffusion coefficients was explore numerically. No strong influence was found indicating that a non-vanishing turbulent field in the parallel direction is less important. However, the latter statement is not true for very strong turbulence in which the turbulent field is much stronger than the mean field (see Hussein & Shalchi 2014). In such cases we find isotropic diffusion meaning that the parallel and perpendicular diffusion coefficients are equal.

Furthermore, the turbulence model used in the current paper is axi-symmetric with respect to the mean magnetic field. Observations (see, e.g, Saur & Bieber 1999 and Narita et al. 2010) and numerical simulations (see, e.g., Dong et al. 2014) have shown that solar wind turbulent spectra are not axi-symmetric. If deviations from axi-symmetry are take into account, the whole diffusion tensor needs to be computed (see, e.g., Weinhorst et al. 2008). It will be subject of future work to present a detailed numerical investigation of test-particle transport in turbulent systems without axi-symmetry.

2.3. The Nonlinear Anisotropic Dynamical Turbulence Model

In order to model dynamical turbulence, one has to specify the dynamical correlation function $\Gamma(\vec{k}, t)$ in Eq. (2). In recent years there has been a more complete understanding of the time scales of turbulence (see, e.g., Matthaeus et al. 1990, Tu & Marsch 1993, Zhou

Table 1: The parameter values used for our test-particle simulations. The values should be appropriate in the interplanetary space at 1 AU heliocentric distance (see, e.g., King 1989).

Parameter	Symbol	Value
2D energy range spectral index	q	2
2D inertial range spectral index	s^{2D}	5/3
Alfvén speed	v_A	33.5 km/s
Slab bendover scale	l_{slab}	0.030 AU
Slab dissipation wavenumber	k_d^{slab}	3×10^5 1/AU
Mean magnetic field	B_0	4.12 nT
Slab fraction	δB_{slab}^2	0.2 δB^2
2D fraction	δB_{2D}^2	0.8 δB^2

Table 2: The different runs performed in the current paper and the values used for the relative turbulence strength $\delta B/B_0$, the slab inertial range spectral index s^{slab}, the dissipation range spectral index p, the ratio of the two bendover scales l_{2D}/l_{slab}, and the two-dimensional dissipation wavenumber k_d^{2D}/k_d^{slab}.

Section	$\delta B/B_0$	s^{slab}	p	l_{2D}/l_{slab}	k_d^{2D}/k_d^{slab}	Figures
1	1	5/3	3	1	1	2-4
2	0.5	5/3	3	1	1	5-7
3	0.75	5/3	3	1	1	8-10
4	0.5	5/3	3, 4, 5	1	1	11-13
5	0.5	5/3	3	0.1	1	14-16
6	0.75	2	3	1	10	17-19
7	0.75	2	3	1	10	20-22

et al. 2004, and Oughton et al. 2006). Based on this improved understanding, Shalchi et al. (2006) have developed the NADT model for the function $\Gamma(\vec{k},t)$. Within the latter model, we have different dynamical correlation functions for slab and two-dimensional modes, respectively.

For the corresponding function of the slab modes we have according to Shalchi et al. (2006)

$$\Gamma^{slab}(k_{\parallel},t) = e^{i\omega_p t-\beta t} \tag{10}$$

where we have used the constant

$$\beta = \sqrt{2}\alpha \frac{v_A}{l_{2D}} \frac{\delta B_{2D}}{B_0} \tag{11}$$

and the plasma wave dispersion relation of shear Alfvén waves

$$\omega_p = j v_A k_\parallel. \tag{12}$$

Obviously one finds an oscillating factor in Eq. (10) describing wave propagation effects. The parameter j used in Eq. (12) indicates the wave propagation direction. Here $j = +1$ is used for forward and $j = -1$ for backward to the ambient magnetic field propagating waves. One would expect that closer to the sun the most waves should propagate forward and far away from the sun the wave intensities should be equal for both directions (see, e.g., Bavassano 2003 for more details). In the current paper we are interested in turbulence parameters at 1 AU heliocentric distance and, thus, we assume that all waves propagate forward and we set $j = +1$. The exponential factor in Eq. (10) contains the decorrelation time scale $\tau = 1/\beta$ where β is given by Eq. (11). The slab component in our model is assumed to experience resonant nonlinear triad interactions with the low-frequency two-dimensional component. Therefore, the time τ is given by the global two-dimensional nonlinear timescale. The parameter α in Eq. (11) is a constant of order one related to the so-called *Karman-Taylor constant* and v_A is the Alfvén speed. In the current paper we set $\alpha = 1$ for simplicity.

For the two-dimensional modes we have according to Shalchi et al. (2006)

$$\Gamma^{2D}(k_\perp, t) = e^{-\gamma t} \tag{13}$$

where we have used

$$\gamma = \gamma(k_\perp) = \beta \begin{cases} 1 & \text{for} \quad k_\perp l_{2D} \leq 1 \\ (k_\perp l_{2D})^{2/3} & \text{for} \quad k_\perp l_{2D} \geq 1 \end{cases} \tag{14}$$

with the constant β defined already in Eq. (11). Obviously no oscillatory factor appears in Eq. (13). For small perpendicular wavenumbers $k_\perp$, we estimate the correlation time as above for the slab modes. For large $k_\perp$, however, the decorrelation time is estimated by using a steady inertial range $k_\perp^{-5/3}$ approximation.

In analytical treatments of the transport, one can directly use the models described here. As pointed out in Hussein & Shalchi (2016), this is not the case in test-particle simulations where a Fourier transformation has to be employed for the dynamical correlation function. We define

$$\chi(\vec{k},\omega) := \frac{1}{\pi}\Re\int_0^\infty dt\ \Gamma(\vec{k},t)e^{-i\omega t}. \tag{15}$$

Using $\chi(\vec{k},\omega)$ instead of $\Gamma(\vec{k},t)$ means that we describe the turbulence in a four-dimensional Fourier space with the coordinates $\vec{k}$ and ω.

In the NADT model, the dynamical correlation function for the slab modes is given by Eq. (10). Therefore, we find

$$\chi^{slab}(\vec{k},\omega) := \frac{1}{\pi}\frac{\beta}{\beta^2+(\omega-\omega_p)^2} \tag{16}$$

where $\omega_p = \omega_p(\vec{k})$ is given by Eq. (12). For the two-dimensional modes, the dynamical correlation function is given by Eq. (13) and, thus

$$\chi^{2D}(\vec{k},\omega) := \frac{1}{\pi}\frac{\gamma}{\gamma^2+\omega^2} \tag{17}$$

where $\gamma = \gamma(\vec{k})$ is given by Eq. (14).

In the next section we explain our numerical approach and in Sect. 4 we show the results for the turbulence model described here.

3. Methodology

We simulate particle transport in dynamical turbulence based on the method described in Hussein & Shalchi (2016). The first step is the creation of turbulence by using the formula

$$\delta\vec{B}(\vec{x},t) = \sqrt{2}\,\delta B \sum_{m=1}^{M}\sum_{n=1}^{N} A\left(k_m,\omega_n\right)\vec{\xi}_m e^{i\left(\vec{k}_m\cdot\vec{x}+\omega_n t+\beta_{mn}\right)} \tag{18}$$

with the random phase β_{mn}. The used method can be seen as an extension of previous simulations performed for either magnetostatic turbulence or undamped propagating plasma waves (see, e.g., Michałek & Ostrowski 1996, Giacalone & Jokipii 1999, Tautz 2010, and Hussein et al. 2015). In the following we describe the parameters and functions used in Eq. (18).

We create two-component turbulence by employing Eq. (18) for slab and two-dimensional modes, respectively and then we add the two obtained magnetic field vectors. For the slab modes and the two-dimensional modes we use the same polarization vector $\vec{\xi}_m$, namely

$$\vec{\xi}_m = (-sin\phi_m, cos\phi_m, 0) \tag{19}$$

where ϕ_m is a random angle.

All quantities used in the code are normalized with respect to the slab bendover scale l_{slab}. This means, for instance, that k_m used above corresponds to the physical quantity $k_\parallel l_{slab}$ or $k_\perp l_{slab}$ and z stands for z/l_{slab}. The frequency ω is normalized with respect to the unperturbed gyro frequency of the particle $\Omega = (qB_0)/(mc\gamma)$ meaning that $\omega_n = \omega/\Omega$. Here we have used the electric charge of the particle q, the rest mass m, the speed of light c, and the Lorentz factor γ.

In Eq. (18) we have also used $\vec{k}_m = k_m \hat{k}_m$ with the random wave unit vector

$$\hat{k}_m = \begin{pmatrix} \sqrt{1-\eta_m^2}\cos\phi_m \\ \sqrt{1-\eta_m^2}\sin\phi_m \\ \eta_m \end{pmatrix}. \tag{20}$$

The random angle ϕ_m was already used in Eq. (19). What the value of η_m is depends on the simulated turbulence model. For the slab modes we have $\eta_m = 1$ and for two-dimensional modes $\eta_m = 0$. In Eq. (18) we have also used the amplitude function

$$A^2(\omega_n, k_m) = \frac{G\left(k_m, \omega_n\right) \Delta k_m \Delta\omega_n}{\sum_{\mu=1}^{M}\sum_{\nu=1}^{N} G(k_\mu, \omega_\nu)\Delta k_\mu \Delta\omega_\nu} \tag{21}$$

where $G(k_\mu, \omega_\nu)$ represents the space-time spectrum

$$G\left(k_m, \omega_n\right) = G(k_m)\chi(k_m, \omega_n). \tag{22}$$

Eqs. (16) and (17) show the functions $\chi(k_m, \omega_n)$ for the NADT model. The function $G(k_m)$ is the usual spectrum as used in simulations of magnetostatic turbulence (see, e.g., Hussein et al. 2015). In the current paper we employ Eq. (6) for the slab modes and Eq. (8) for the two-dimensional modes.

In the used model for $\chi(k_m, \omega_n)$, one finds the Alfvén speed v_A which can be normalized with respect to the particle speed v so that

$$\frac{v_A}{v} = \frac{v_A}{c}\frac{\sqrt{R_0^2 + R^2}}{R}. \tag{23}$$

Here we have used the parameter

$$R_0 = \frac{1}{l_{slab} B_0} \begin{cases} 0.511\text{MV} & \text{for} \quad \text{electrons} \\ 938\text{MV} & \text{for} \quad \text{protons}, \end{cases} \tag{24}$$

and the dimensionless rigidity defined via $R = R_L/l_{slab}$ where $R_L = v/\Omega$ is the unperturbed Larmor radius. For $l_{slab} = 0.03$AU and $B_0 = 4.12$nT this gives $R_0 = 9.2 \times 10^{-5}$ for electrons

and $R_0 = 0.169$ for protons. All other parameter values used in our simulations are listed in Tables 1 and 2 .

In our test-particle simulations in dynamical turbulence we have to deal with the same problems one has to deal with in simulations of static turbulence (see again Hussein et al. (2015) for more details). For dynamical turbulence, however, there are a few additional concerns. We need a certain number of grid points in space and time. For most of our runs we have set $N = M = 256$ in Eq. (18). For lower rigidities we had to set $N = M = 64$ to avoid too long computation times. In all runs we have computed running diffusion coefficients for times up to at least $\Omega t = 10^4$ (here Ω denotes again the unperturbed gyro frequency) to ensure that we are in the stable regime.

Furthermore, as noted in Hussein & Shalchi (2016), the value of the minimum frequency ω_{min} has a strong influence on the obtained parallel and perpendicular mean free paths. This influence was noticed for both protons and electrons but was much stronger for electrons. To avoid this problem, we performed our simulations for small enough values of ω_{min}.

Following the ideas presented in Tautz (2010), we also compute the errors of the different mean free paths. The latter author noted that using the standard deviation as a mean of estimating the error is inappropriate as the mean square displacement calculated in the Monte Carlo code is the variance of the distribution function for the diffusion equation itself. In addition, test particles interacting with turbulent magnetic fields scatter in a random manner leading to a huge variance in their square deviation. Hence one has to come up with a method that takes into account the averaging processes used over the number of turbulence manifestations, N_T, for each of which a fixed number of test particles were simulated in space and time resulting a diffusion coefficient. The mean error is then defined to be the deviation of the different mean free paths λ_n from the final averaged mean free

path λ_f. Mathematically this reads

$$\begin{aligned}\sigma_\lambda^2 &= \frac{1}{N_T-1} \\ &\times \left\{\sum_{n=0}^{N_T}(\lambda_n-\lambda_f)^2-\frac{1}{N_T}\Big[\sum_{n=0}^{N_T}(\lambda_n-\lambda_f)\Big]^2\right\}. \end{aligned} \tag{25}$$

Using Eq. (25), both the error in parallel and perpendicular mean free paths where calculated, $\Delta\lambda_\parallel$ and $\Delta\lambda_\perp$ respectively. To calculate the error in the ratio of the two mean free paths, $\lambda_\perp/\lambda_\parallel$, we use the rule of error combination

$$\Delta\Big(\frac{\lambda_\perp}{\lambda_\parallel}\Big)=\Big(\frac{\Delta\lambda_\perp}{\lambda_\perp}+\frac{\Delta\lambda_\parallel}{\lambda_\parallel}\Big)\frac{\lambda_\perp}{\lambda_\parallel}. \tag{26}$$

In most plots shown in Sect. 4 we have included the error bars based on the method presented here.

4. Results

In Tables 1 and 2 we show the different parameters used in our simulation runs. In the following we vary the magnetic field ratio $\delta B/B_0$, the dissipation range spectral index p, the ratio of the bendover scales l_{2D}/l_{slab}, the inertial range spectral index of the slab modes s^{slab}, as well as the dissipation wavenumber of the two-dimensional modes k_d^{2D}.

4.1. Slab/2D Turbulence with $\delta B/B_0 = 1.0$

Often one assumes that the ratio of turbulent and mean magnetic field is $\delta B/B_0 = 1.0$ (see, e.g., Bieber et al. 1994 and Bieber et al. 1996). Furthermore, we assume equal turbulence bendover scales $l_{2D} = l_{slab}$ and set the dissipation range spectral index to $p = 3$. We vary the particle rigidity from usually a few percent megavolt up to about 50 gigavolt. We compute the parallel mean free path, the perpendicular mean free path, as well as the

ratio of the two diffusion parameters $\lambda_\perp/\lambda_\parallel$. Our numerical findings are visualized in Figs. 2, 3, and 4. All results are compared with different measurements performed in the solar system.

Qualitatively, our results are similar compared to the simulations presented in Hussein & Shalchi (2016) which were obtained for the *damping model of dynamical turbulence* and the *random sweeping model*. As in previous work we conclude that the obtained parallel mean free paths are too small compared to the Palmer (1982) consensus range. Therefore, we change different parameters in our test-particle code to explore their influence on the different diffusion parameters. This is done in the following paragraphs.

4.2. Slab/2D Turbulence with $\delta B/B_0 = 0.5$

In Hussein & Shalchi (2016) it was shown that the simulated parallel mean free path is too small if the magnetic field ratio is assumed to be $\delta B/B_0 = 1$. Therefore, the latter ratio was changed to $\delta B/B_0 = 0.5$ as suggested in Ruffolo et al. (2012). In the current paragraph we do the same in the context of the NADT model and we show our findings for the different diffusion parameters in Figs. 5, 6, and 7.

As expected we find an increased parallel mean free path but a smaller perpendicular mean free path. The former transport coefficient goes directly through the Palmer (1982) consensus range confirming that we can indeed reproduce solar wind observations of energetic particles numerically. The perpendicular diffusion coefficients, however, are now too small. The same applies for the ratio of the two diffusion parameters $\lambda_\perp/\lambda_\parallel$.

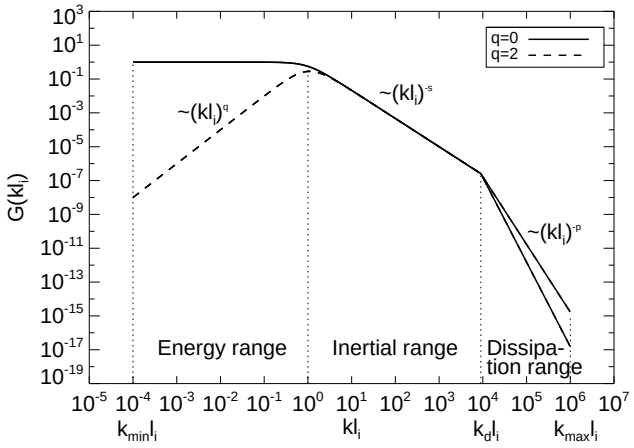

Fig. 1.— The spectra used in the current paper for the slab modes ($q = 0$) and the two-dimensional modes ($q = 2$).

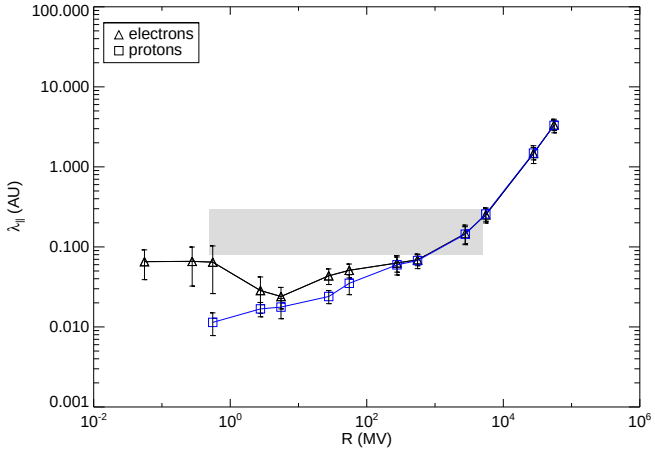

Fig. 2.— The parallel mean free path versus magnetic rigidity for two-component turbulence, the NADT model, and $\delta B/B_0 = 1.0$. The shaded band represents the Palmer (1982) consensus range.

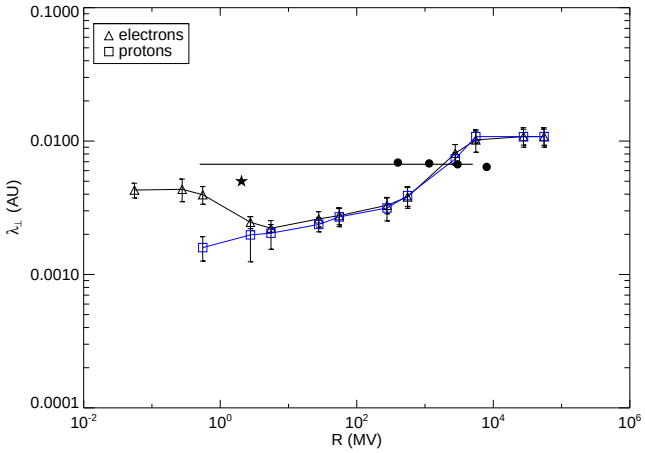

Fig. 3.— The perpendicular mean free path versus magnetic rigidity for two-component turbulence, the NADT model, and $\delta B/B_0 = 1.0$. For comparison we show observations of Jovian electrons (Chenette et al. 1977, star), Ulysses measurements of Galactic protons (Burger et al. 2000, dots), and the Palmer (1982) value (horizontal line).

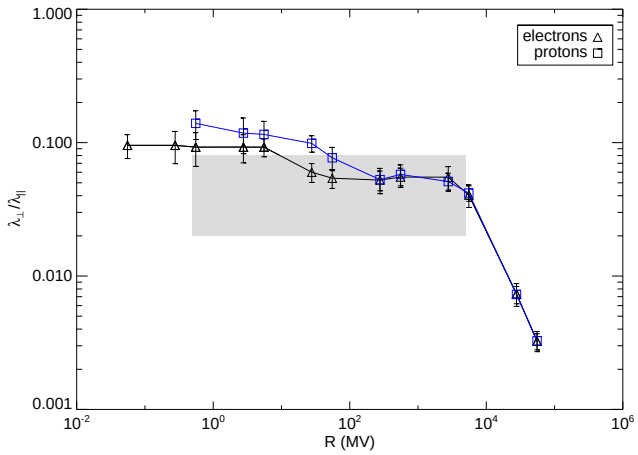

Fig. 4.— The ratio of perpendicular and parallel mean free paths versus magnetic rigidity for two-component turbulence, the NADT model, and $\delta B/B_0 = 1.0$. The shaded band represents the Palmer (1982) consensus range.

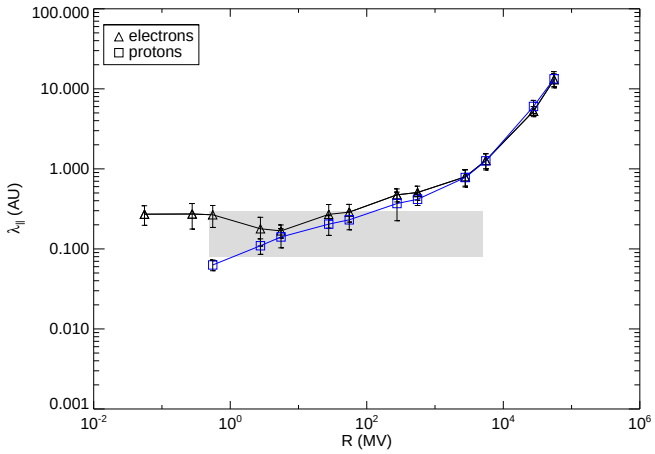

Fig. 5.— Caption is exactly as in Fig. 2 but results were obtained for $\delta B/B_0 = 0.5$.

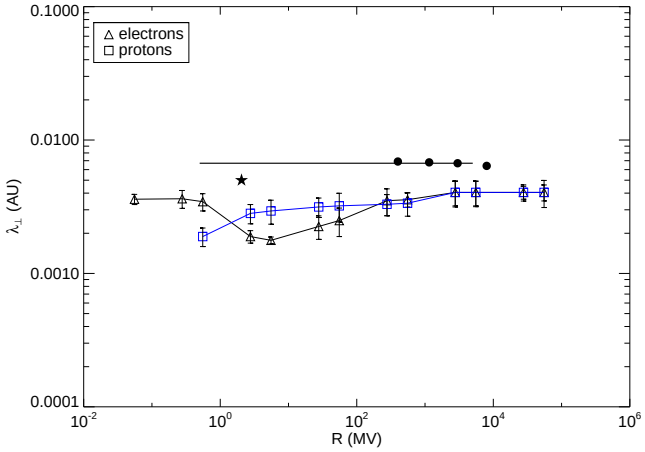

Fig. 6.— Caption is exactly as in Fig. 3 but results were obtained for $\delta B/B_0 = 0.5$.

4.3. Slab/2D Turbulence with $\delta B/B_0 = 0.75$

Above we have performed the simulations for the magnetic field ratios $\delta B/B_0 = 1$ and $\delta B/B_0 = 0.5$. According to Fig. 2 the parallel mean free path is too short for $\delta B/B_0 = 1$. For a reduced magnetic field ratio of $\delta B/B_0 = 0.5$ the parallel mean free path is much larger but is still within the Palmer (1982) consensus range (see Fig. 5). In the current paragraph we show the simulations performed for an intermediate turbulence level of $\delta B/B_0 = 0.75$. The obtained diffusion parameters are visualized in Figs. 8, 9, and 10.

As expected, the parallel mean free path for electrons is now perfectly inside the box representing the solar wind observations. The perpendicular mean free path as well as the ratio of the two diffusion coefficients is close to the different observations as well. Obviously, the magnetic field ratio is a critical parameter controlling both spatial diffusion coefficients. This is exactly what one expects and what is also predicted by analytical investigations of the transport (see, e.g., Shalchi 2009 and Shalchi 2015). For $\delta B/B_0 = 0.75$ we find the best agreement between simulations and observations.

4.4. Influence of the Dissipation Range Spectral Index

Above, as well as in Hussein & Shalchi (2016), the dissipation range spectral index was set to $p = 3$. This is a numerical value which is close to solar wind observations of magnetic turbulence (see, e.g., Denskat & Neubauer 1982). It is expected that the smallest scales of turbulence, corresponding to the dissipation range, influence the parallel mean free path at low rigidities due to the gyroresonant interactions between particles and turbulence.

In Figs. 11, 12, and 13 we show the diffusion parameters for $p = 3$, $p = 4$, and $p = 5$. Obviously there is almost no influence of the dissipation range spectral index on the considered transport parameters.

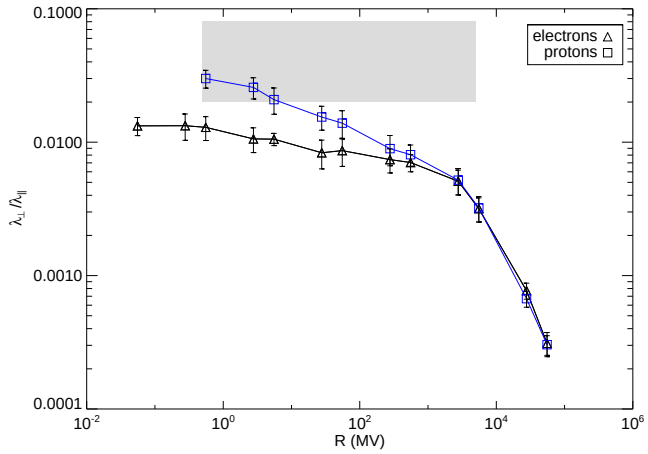

Fig. 7.— Caption is exactly as in Fig. 4 but results were obtained for $\delta B/B_0 = 0.5$.

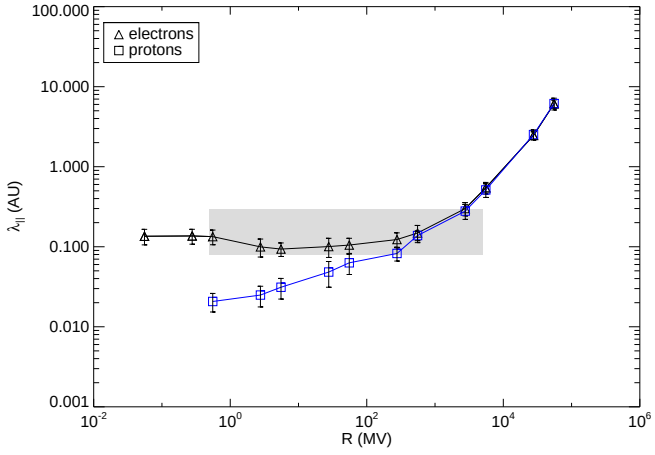

Fig. 8.— Caption is exactly as in Fig. 2 but results were obtained for $\delta B/B_0 = 0.75$.

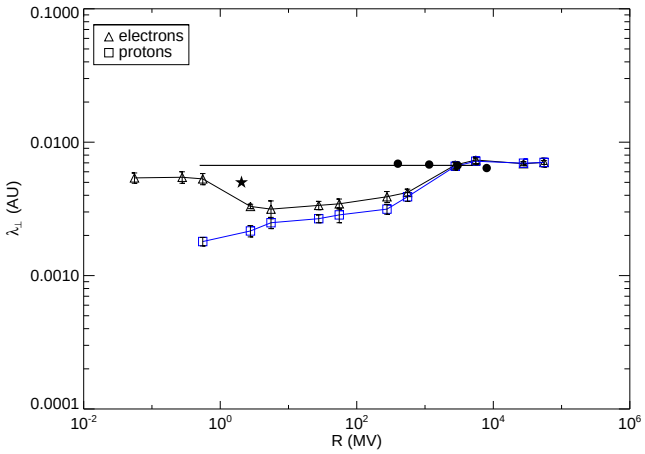

Fig. 9.— Caption is exactly as in Fig. 3 but results were obtained for $\delta B/B_0 = 0.75$.

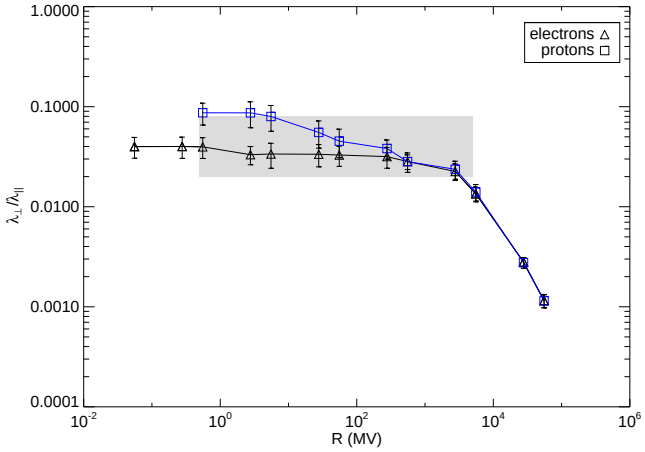

Fig. 10.— Caption is exactly as in Fig. 4 but results were obtained for $\delta B/B_0 = 0.75$.

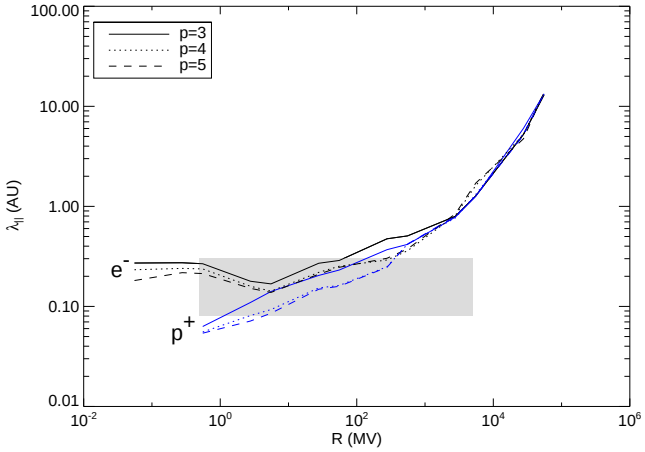

Fig. 11.— The parallel mean free path versus magnetic rigidity for two-component turbulence, the NADT model, and $\delta B/B_0 = 0.5$. We have shown results for different values of the dissipation range spectral index p. The shaded band represents the Palmer (1982) consensus range.

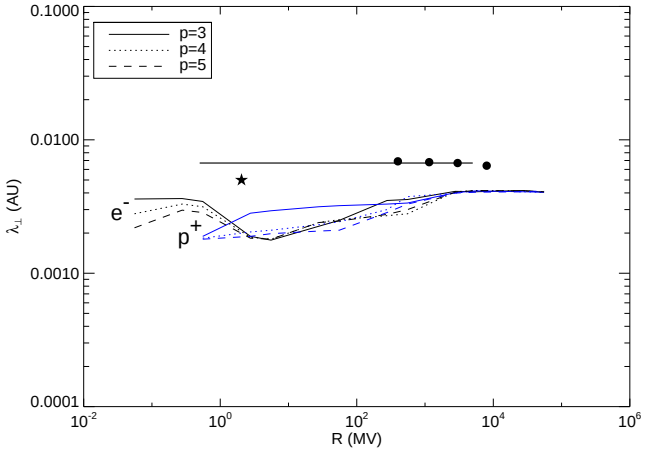

Fig. 12.— The perpendicular mean free path versus magnetic rigidity for two-component turbulence, the NADT model, and $\delta B/B_0 = 0.5$. We have shown results for different values of the dissipation range spectral index p. For comparison we show observations of Jovian electrons (Chenette et al. 1977, star), Ulysses measurements of Galactic protons (Burger et al. 2000, dots), and the Palmer (1982) value (horizontal line).

4.5. Influence of the Two-dimensional Bendover Scale

Another parameter which can be changed in our simulations, is the bendover scale of the two-dimensional modes l_{2D}. The latter parameter denotes the turnover from the intermediate scales of the inertial range to the large scales of the energy range. Originally it was assumed that $l_{2D} = 0.1 l_{slab}$, at least in the context of test-particle calculations (see again Bieber et al. 1994). In recent years, the ratio of the two bendover scales was changed to $l_{2D} = l_{slab}$ (see, e.g., Hussein & Shalchi 2016) and this is what we have used above.

In Figs. 14, 15, and 16 we show diffusion parameters for $l_{2D} = 0.1 l_{slab}$. We can see that the parallel mean free path as well as the perpendicular mean free path are drastically reduced due to the smaller values of l_{2D}. Clearly we find that the perpendicular mean free path is far away from the different interplanetary measurements. The parallel mean free path, however, is now directly in the Palmer (1982) consensus range. The ratio $\lambda_\perp/\lambda_\parallel$ is too small as well.

4.6. Influence of the Dissipation Scales

Simulations of MHD turbulence in presence of a mean field display anisotropic power in the parallel and perpendicular direction. In simulations the dissipative range is reached at different scales. The measure of the two-dimensional correlations and of the Taylor scale in the solar wind (see Weygand et al. 2011) also support the existence of different dissipative scales in the parallel and perpendicular directions. This corresponds to different dissipation wavenumbers k_d^{2D} and k_d^{slab}.

In order to test the influence of the dissipation scales on the diffusion of energetic particles, we repeat one set of simulations with a higher value of the dissipation wavenumber of the two-dimensional modes k_d^{2D}. Above we have used $k_d = 3 \times 10^5 1/AU$ in all of

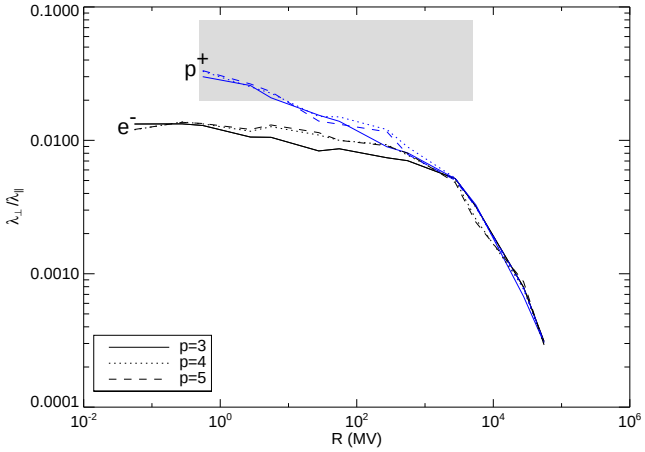

Fig. 13.— The ratio of perpendicular and parallel mean free paths versus magnetic rigidity for two-component turbulence, the NADT model, and $\delta B/B_0 = 0.5$. We have shown results for different values of the dissipation range spectral index p. The shaded band represents the Palmer (1982) consensus range.

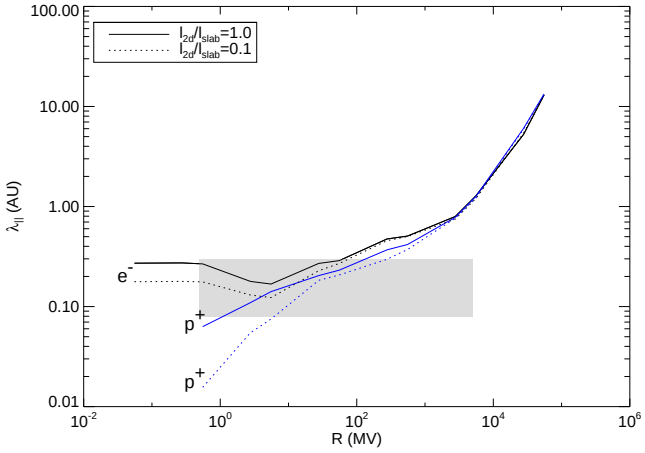

Fig. 14.— The parallel mean free path versus magnetic rigidity for two-component turbulence, the NADT model, and $\delta B/B_0 = 0.5$. We have shown results for different values of the two-dimensional bendover scale l_{2D}. The shaded band represents the Palmer (1982) consensus range.

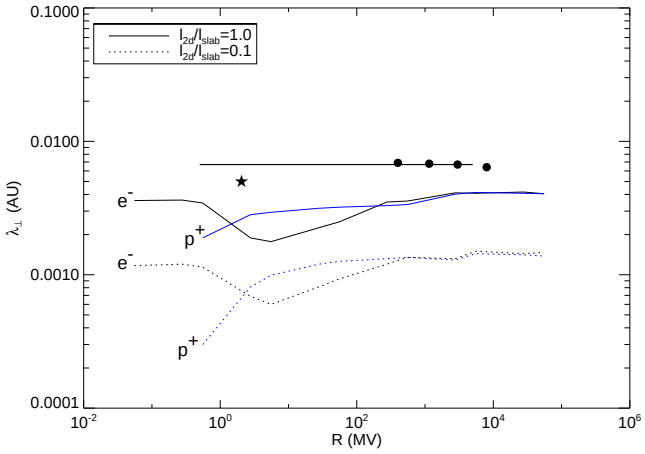

Fig. 15.— The perpendicular mean free path versus magnetic rigidity for two-component turbulence, the NADT model, and $\delta B/B_0 = 0.5$. We have shown results for different values of the two-dimensional bendover scale l_{2D}. For comparison we show observations of Jovian electrons (Chenette et al. 1977, star), Ulysses measurements of Galactic protons (Burger et al. 2000, dots), and the Palmer (1982) value (horizontal line).

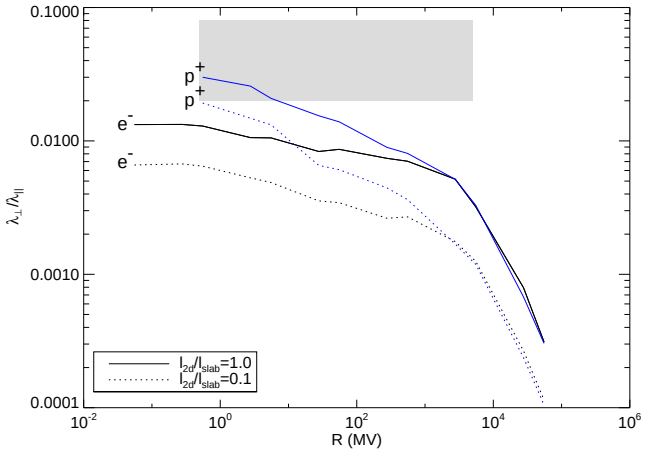

Fig. 16.— The ratio of perpendicular and parallel mean free paths versus magnetic rigidity for two-component turbulence, the NADT model, and $\delta B/B_0 = 0.5$. We have shown results for different values of the two-dimensional bendover scale l_{2D}. The shaded band represents the Palmer (1982) consensus range.

our simulations for both slab and the two-dimensional modes. We redo the set with $\delta B/B_0 = 0.75$, $l_{2D} = l_{slab}$, and $p = 3$ keeping the slab dissipation wavenumber as is but use $k_d^{2D} = 3 \times 10^6 1/AU$. Figs. 17, 18, and 19 show the parallel mean free path, the perpendicular mean free path, and the ratio of the two mean free paths as function of rigidity for the different values of k_d^{2D}. Clearly, the value of k_d^{2D} has no noticeable influence on the transport parameters.

4.7. Influence of the Inertial Range Spectral Index

In the local description of turbulence the parallel and perpendicular spectral indexes differ substantially (see, e.g., Goldreich & Shridar 1995, Cho & Vishniac 2000, and Boldyrev 2005) and this has been confirmed by solar wind measurements (see, e.g., Horbury et al. 2008). To test the influence of a varying inertial range spectral index s on the transport of energetic particles, we perform one set of simulations with $s^{slab} = 2$ for the slab modes and keep $s^{2D} = 5/3$ for the two-dimensional modes. As before, we use $\delta B/B_0 = 0.75$, $l_{2D} = l_{slab}$, and $p = 3$. Figs. 20, 21, and 22 show the parallel mean free path, the perpendicular mean free path, and the ratio of the two mean free paths as function of rigidity for the different values of s^{slab}. Clearly, a steeper inertial range for the slab modes has no noticeable influence on the transport parameters.

5. Summary and Conclusion

The current paper is a sequel of Hussein & Shalchi (2016) where we have started to perform test-particle simulations for dynamical turbulence. The turbulence dynamics can have a strong influence on particle diffusion coefficients at low particle rigidities. In the previous work, we have employed two models for dynamical turbulence, namely the

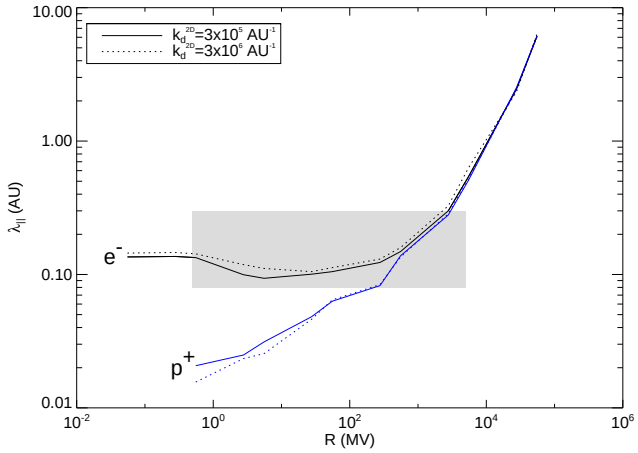

Fig. 17.— The parallel mean free path versus magnetic rigidity for composite turbulence using the NADT model with $\delta B/B_0 = 0.75$, $l_{2D}/l_{slab} = 1.0$, and $p = 3$ for different values of k_d^{2D}. The shaded band represents the Palmer (1982) consensus range.

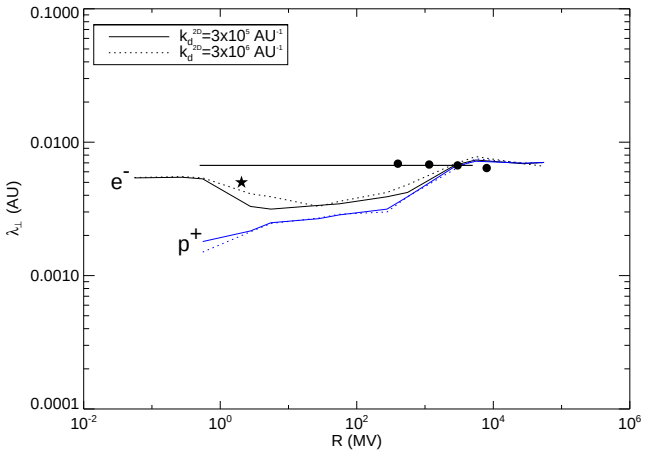

Fig. 18.— The perpendicular mean free path versus magnetic rigidity for composite turbulence using the NADT model with $\delta B/B_0 = 0.75$, $l_{2D}/l_{slab} = 1.0$ and $p = 3$ for different values of k_d^{2D}. We show observations of Jovian electrons (star), Ulysses measurements of Galactic protons (dots), and the Palmer (1982) value (horizontal line).

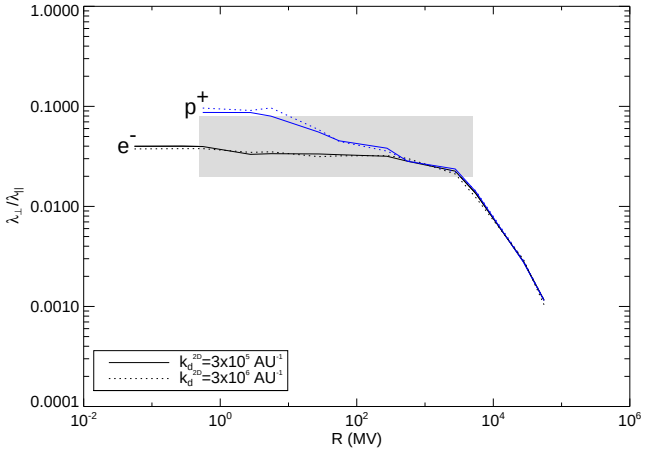

Fig. 19.— The ratio of perpendicular to parallel mean free paths versus magnetic rigidity for composite turbulence using the NADT model with $\delta B/B_0 = 0.75$, $l_{2D}/l_{slab} = 1.0$, and $p = 3$ for different values of k_d^{2D}. The shaded band represents the Palmer (1982) consensus range.

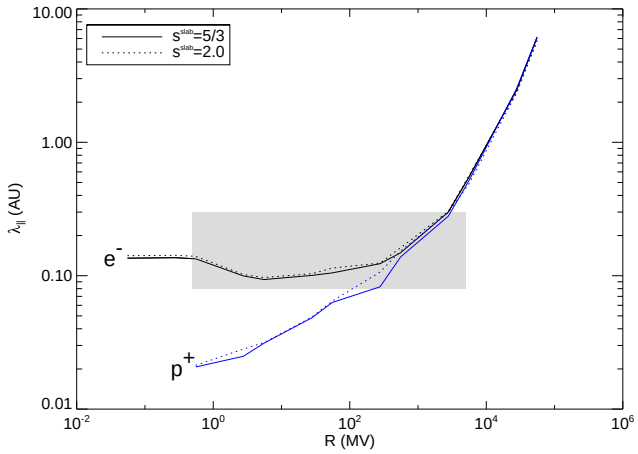

Fig. 20.— The parallel mean free path versus magnetic rigidity for composite turbulence using the NADT model with $\delta B/B_0 = 0.75$, $l_{2D}/l_{slab} = 1.0$, and $p = 3$ for different values of s^{slab}. The shaded band represents the Palmer (1982) consensus range.

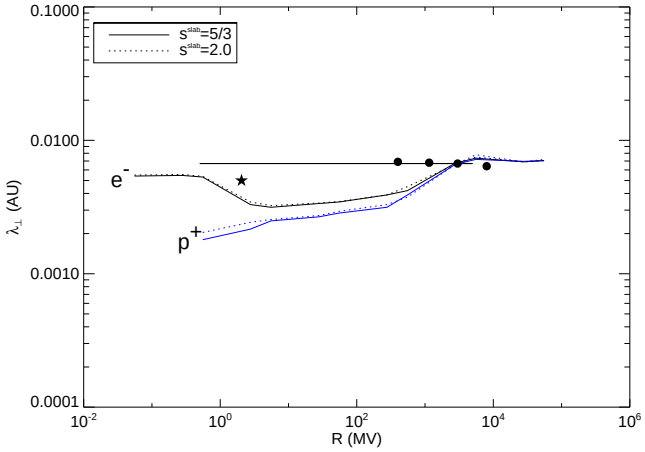

Fig. 21.— The perpendicular mean free path versus magnetic rigidity for composite turbulence using the NADT model with $\delta B/B_0 = 0.75$, $l_{2D}/l_{slab} = 1.0$ and $p = 3$ for different values of s^{slab}. We show observations of Jovian electrons (star), Ulysses measurements of Galactic protons (dots), and Palmer (1982) value (horizontal line).

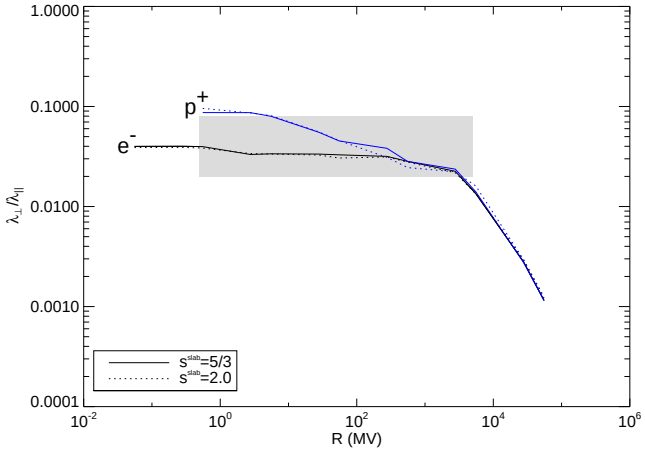

Fig. 22.— The ratio of perpendicular to parallel mean free paths versus magnetic rigidity for composite turbulence using the NADT model with $\delta B/B_0 = 0.75$, $l_{2D}/l_{slab} = 1.0$, and $p = 3$ for different values of s^{slab}. The shaded band represents the Palmer (1982) consensus range.

damping model of dynamical turbulence and the *random sweeping model*. Both models were originally proposed in the pioneering work of Bieber et al. (1994).

It is the purpose of the current paper to replace the aforementioned dynamical turbulence models by the so-called *Nonlinear Anisotropic Dynamical Turbulence (NADT) model* of Shalchi et al. (2006) which takes into account wave propagation effects as well as damping effects. Furthermore, we perform a detailed parameter study in order to explore the influence of the magnetic field ratio $\delta B/B_0$, the turbulence scale ratio l_{2D}/l_{slab}, the dissipation range spectral index p, the dissipation wavenumber k_d, as well as the inertial range spectral index s on the parallel mean free path $\lambda_\parallel$, the perpendicular mean free path $\lambda_\perp$, and the ratio of the two diffusion parameters $\lambda_\perp/\lambda_\parallel$. Our findings are shown in Figs. 2-22 and the corresponding parameter values are listed in Tables 1 and 2.

We found that the influence of the dissipation range spectral index is minor. The influence of the inertial range spectral index and the dissipation scales are negligible as well. The magnetic field ratio, on the other hand, has a strong influence on both diffusion coefficients and their ratio. We found best agreement with the Palmer (1982) consensus range for $\delta B/B_0 = 0.75$ (corresponding to approximately $\delta B^2/B_0^2 = 0.6$) which is between the values $\delta B/B_0 = 0.5$ and $\delta B/B_0 = 1$ usually used for this type of work. We also found that the ratio of the bendover scales l_{2D}/l_{slab} has an influence on the parallel mean free path and a very strong influence on the perpendicular diffusion coefficient. This was predictable because analytical treatments of the transport (see, e.g., Shalchi 2015) show the importance of the so-called *Kubo number* on the perpendicular motion of energetic particles. The latter number depends on the magnetic field ratio as well as the turbulence scales.

The main conclusion of the current paper is that we can indeed reproduce different solar wind observations performed for energetic particles interacting with magnetic turbulence if we employ the NADT model. More detailed turbulence measurements would show what

the exact value of the different parameters used in the current paper are. Then one could draw more conclusions concerning the validity of the employed turbulence model.

A. Shalchi acknowledges support by the Natural Sciences and Engineering Research Council (NSERC) of Canada. Most simulations shown in this article were obtained by using the national computational facility provided by WestGrid. We are also grateful to S. Safi-Harb for providing her CFI-funded computational facilities for code tests and for some of the simulation runs presented here.

REFERENCES

Alexandrova, O., Carbone, V., Veltri, P., & Sorriso-Valvo, L. 2008, ApJ, 674, 1153

Bavassano, B. 2003, AIP Conference Proceedings, 679, 377

Belcher, J. W., & Davis Jr., L. 1971, JGR, 76, 3534

Bieber, J. W., Matthaeus, W. H., Smith, C. W., Wanner, W., Kallenrode, M.-B., & Wibberenz, G. 1994, ApJ, 420, 294

Bieber, J. W., Wanner, W., & Matthaeus, W. H. 1996, JGR, 101, 2511

Boldyrev, S. 2005, ApJ, 626, L37

Burger, R. A., Potgieter, M. S., & Heber, B. 2000, JGR, 105, 27447

Chenette, D. L., Conlon, T. F., Pyle, K. R., & Simpson, J. A. 1977, ApJ, 215, L95

Cho, J. & Vishniac, E. T. 2000, ApJ, 539, 273

Denskat, K. U. & Neubauer, F. M. 1982, Observations of hydrodynamik turbulence in the solar wind. *In Solar Wind Five, (Ed.) Neugebauer, M., Proceedings of a conference held in Woodstock, Vermont, November 1-5, 1982, vol. 2280 of NASA Conference Publication, pp. 81-91, NASA, Washington, U.S.A*

Dong, Y., Verdini, A., & Grappin, R. 2014, ApJ, 793, 118

Giacalone, J., & Jokipii, J. R. 1999, ApJ, 520, 204

Goldreich, P. & Sridhar, S. 1995, ApJ, 438, 763

Horbury, T. S., Forman, M., & Oughton, S. 2008, PRL, 101, 175005

Howes, G. G., Dorland, W., Cowley, S. C., Hammett, G. W., Quataert, E., Schekochihin, A. A., & Tatsuno, T. 2008, 100, 065004

Hussein, M. & Shalchi, A. 2014, ApJ, 785, 31

Hussein, M., Tautz, R., & Shalchi, A. 2015, JGR, 120, 4095

Hussein, M. & Shalchi, A. 2016, ApJ, 817, 136

King, J. H. 1989, Interplanetary medium data book, supplement 4, 1985-1988

Matthaeus, W. H., Goldstein, M. L., & Roberts, D. A. 1990, JGR, 95, 20673

Matthaeus, W. H., Ghosh, S., Oughton, S., & Roberts, D. 1996, JGR, 101, 7619

Matthaeus, W. H., Bieber, J. W., Ruffolo, D., Chuychai, P., & Minnie, J. 2007, ApJ, 667, 956

Michałek, G., & Ostrowski, M. 1996, Nonlin. Proc. Geophys., 3, 66

Narita, Y., Glassmeier, K.-H., Sahraoui, F., & Goldstein, M. L. 2010, PRL, 104, 171101

Osman, K. T., & Horbury, T. S. 2009a, JGR, 114, A06103

Osman, K. T., & Horbury, T. S. 2009b, Annales Geophysicae, 27, 3019

Oughton, S., Priest, E. R., & Matthaeus, W. H. 1994, J. Fluid. Mech., 280, 95

Oughton, S., Dmitruk, P., & Matthaeus, W. H. 2006, Phys. Plasmas, 13, 042306

Palmer, I. D. 1982, Rev. Geophys. Space Phys., 20, 335

Qin, G., Matthaeus, W. H., & Bieber, J. W. 2002a, GeoRL, 29, 1048

Qin, G., Matthaeus, W. H., & Bieber, J. W., 2002b, ApJ, 578, L117

Ruffolo, D., Pianpanit, T., Matthaeus, W. H., & Chuychai, P. 2012, ApJ, 747, L34

Saur, J. & Bieber, J. W. 1999, JGR, 104, 9975

Schlickeiser, R., 2002, Cosmic Ray Astrophysics (Berlin: Springer)

Shaikh, D., & Zank, G. P. 2007, ApJ, 656, L17

Shalchi, A., Bieber, J. W., Matthaeus, W. H., & Schlickeiser, R. 2006, ApJ, 642, 230

Shalchi, A. 2009, Nonlinear Cosmic Ray Diffusion Theories (Astrophysics and Space Science Library, Vol. 362; Berlin: Springer)

Shalchi, A., & Weinhorst, B. 2009, AdSpR, 43, 1429

Shalchi, A. 2015, PhPl, 22, 010704

Tautz, R. C. 2010, Comput. Phys. Commun., 181, 71

Tautz, R. C., & Shalchi, A. 2013, JGR, 118, 642

Tu, C.-Y. & Marsch, E. 1993, JGR, 98, 1257

Turner, A. J., Gogoberidze, G., & Chapman. S. C. 2012, PhRvL, 108, 8

Weinhorst, B., Shalchi, A., & Fichtner, H. 2008, ApJ, 677, 671

Weygand, J. M., Matthaeus, W. H., Dasso, S., & Kivelson, M. G. 2011, Journal of Geophysical Research (Space Physics), 116, A08102

Zank, G. P., & Matthaeus, W. H. 1993, Physics of Fluids A, 5, 257

Zhou, Y., Matthaeus, W. H., & Dmitruk, P. 2004, Rev. Mod. Phys., 76, 1015

This manuscript was prepared with the AAS LaTeX macros v5.2.